# Manipulating the Phase Morphology in PPS/PA66 Blends Using Clay

**Hao Zou, Nanying Ning, Run Su, Qin Zhang, Qiang Fu**

*Department of Polymer Science and Materials, State Key Laboratory of Polymer Materials Engineering, Sichuan University, Chengdu 610065, China*

Received 25 January 2006; accepted 20 May 2007
DOI 10.1002/app.26880
Published online 25 July 2007 in Wiley InterScience (www.interscience.wiley.com).

**ABSTRACT:** By adding a small amount of clay into poly(*p*-phenylene sulfide) (PPS)/polyamide 66 blends, the morphology was found to change gradually from sea–island into cocontinuity and lamellar supramolecular structure, as increasing of clay content. Clay was selectively located in the PA66 phase, and the exfoliated clay layers formed an edge-contacted network. The change of morphology is not caused by the change of volume ratio and viscosity ratio but can be well explained by the dynamic interplay of phase separation between PPS and PA66 through preferential adsorption of PA66 onto the clay layers and through layer–layer repulsion. This provides a means of manipulating the phase morphology for the immiscible polymer blends. The mechanical and tribological properties of PPS/PA66 blends with different phase morphologies (different clay contents) were studied. Both tensile and impact strength of the blends were found obviously increased by the addition of clay. The antiwear property was greatly improved for the blends with cocontinuous phase form. Our work indicates that the phase-separating behavior of polymer blends contained interacting clay can be exploited to create a rich diversity of new structures and useful nanocomposites. © 2007 Wiley Periodicals, Inc. J Appl Polym Sci 106: 2238–2250, 2007

**Key words:** poly(*p*-phenylene sulfide); polyamide 66; blends; clay; morphology

## INTRODUCTION

During the last decades, synthesizing polymer/clay nanocomposites has been an important path to tailor properties of polymeric materials because of their potential industrial applications.[1–4] In the recent years, a growing interest has focused on the ternary polymer/polymer/clay composites.[5–11] Because of its high aspect ratio and high surface area, clay can affect efficiently the phase morphology of polymer blends. Wang et al.[5] reported a decreased domain size in polystyrene/polypropylene (PP) blend by the addition of clay and attributed it to the fact that two immiscible polymer chains might coexist together between the intercalated clay platelets acting as block (or graft) copolymers. Ray and Bousmina[6] described the compatibilization efficiency of organically modified montmorillonite (OMMT) in the immiscible polycarbonate/poly(methyl methacrylate) blends, and Mehrabzadeh and Kamal observed not only a reduced dispersed phase but also a change from spherical to laminar shape in the high-density polyethylene/polyamide6 blends by adding 5 wt % clay into the blends.[7] Lee et al.[8] found that for the 80/20 (w/w) polyamide6/ERP blend, the dispersed domain size of EPR phase in the N6 matrix decreased significantly even if a small amount of clay was added. And the exfoliated clay plates effectively prevented the coalescence of the dispersed domains. Feng et al.[9] found that in PP and polyamide6/clay nanocomposites (NPA6) system, at the low clay contents (3, 5 wt %), NPA6 exhibited continuous lamellar structure in PP matrix, as pristine PA6 did in PP/PA6 blend, but at a higher clay content (10 wt %) only ellipsoids or elongated ellipsoids were observed. Li and Shimizu[10] reported a significantly decreased domain size in the poly(phenylene oxide) (PPO)/polyamide6 blend by adding 2% clay, but a cocontinuous morphology by adding 5% clay. They owned it to the change of the viscosity ratio at higher clay content.[10] A similar cocontinuous morphology was found in polyamide6/acrylonitrile-butadiene-styrene (ABS) nanocomposites.[11] Moreover, Rafailovich et al.[12] developed a means to prepare

*Correspondence to:* Q. Fu (qiangfu@scu.edu.cn).
Contract grant sponsor: National Natural Science Foundation of China; contract grant number: 50373030 and 50533050.
Contract grant sponsor: National Natural Science Foundation of China; contract grant number: 20404008.
Contract grant sponsor: Special Funds for Major State Basic Research Projects of China; contract grant number: 2003CB615600.
Contract grant sponsor: Ministry of Education of China; contract grant number: 104154.

thin films of immiscible polymer blends using organoclay as compatibilizer.

Poly(*p*-phenylene sulfide) (PPS) possesses high temperature resistance combined with good mechanical properties, exceptional chemical and solvent resistance, high dimensional stability, and good processability.[13,14] It is widely used in the fields of automotive, industrial, and consumer goods sectors. It is, however, rather brittle with a low elongation at break and also high cost. Thus, blending PPS with other polymers for good mechanical properties and cheap price is very common. Among them, polyamide66 (PA66) is a widely used engineering plastic.[15] It possesses an outstanding combination of properties such as low density, easy processing, good strength, and solvent resistance. More importantly, it was found that PA66 has a superior wear resistance compared with other polymers, and its friction coefficient was affected greatly by normal load, sliding speed, and temperature.[16–19] PPS has a high friction coefficient and wear resistance because it does not form a strong transfer film on a metal counter face.[20] To improve the tribological properties of PPS, Chen et al. have blended PA66 with PPS to obtain the polymer blends with good mechanical and tribological properties.[21] They concluded that the friction coefficient of the blends was governed by the PA66 melting properties under action of the thermal control of friction, while the adhesion between the PPS and steel surface was the major factor influencing wear. Unfortunately, PPS has no thermodynamic miscibility with PA66, and thus the blends often have a coarse heterogeneous phase structure with low adhesion between the components. Usually, the interfacial interactions are enhanced by use of a functionalized modifier, and addition or *in situ* formation of a block/graft copolymer, the blocks of which have the same or similar chemical composition as the homopolymers in their immiscible blend.

In this article, we introduced that a small amount of clay into the PPS/PA66 system to manipulate the phase morphology and investigated the effect of phase morphology on the mechanical and tribological property of PPS/PA66 blends at a fixed ratio (PPS/PA66 = 60/40). The morphology was found to change gradually from sea–island to cocontinuity and finally to lamellar supramolecular structure, as increasing of clay content. In this way, if we ignore the effect of clay, the relationship between phase morphology and triblogical property can be well studied. We reported here such a result and demonstrated how the triblogical property could be improved by just only changing the phase morphology. The friction and wear mechanisms are discussed in terms of the morphology and formation of transfer films.

## EXPERIMENTAL

### Materials

PPS in a powder form ($M_w$ = 48,000, melting temperature = 285°C) was purchased from Sichuan Deyang Science. Polyamide66 (PA66) ($M_w$ = 20,000, melting temperature = 250°C) came from Shenma Company. Organically modified clay with a cation-exchanged capacity of 100 meq/100 g was prepared using an alkylammonium salt, dioctadecyl dimethylammouium bromide (2C-18).

### Blend preparation

Clay (powder form), PPS, and PA 66 were first dry mixed by home mixer. Melt blending of PPS/PA66 with fixed composition (60/40) with different contents of organic clay or untreated clay was conducted using a twin-screw extruder (TSSJ-25, Chen-Guang, Chengdu, China) at 180–290°C. The screw speed was 120 rpm. Blend loaded without clay was also prepared by melt extrusion in the same manner individually. The extruded strands were then pelletized and dried at 85°C. The resulting pellets were injected in PS40E5ASE (NISSEI, Tokyo, Japan) at 275–300°C. The reference of sample was listed in Table I.

**TABLE I**
**Sample Reference Used in the Experiment**

| Reference | PPS (wt %) | PS66 (wt %) | Organically modified clay (phr*) | Untreated clay (phr*) | Morphology of the blends |
|---|---|---|---|---|---|
| 1 | 60 | 40 | 0 | \ | Sea–island |
| 2 | 60 | 40 | 1 | \ | Cocontinuous |
| 3 | 60 | 40 | 5 | \ | Cocontinuous |
| 4 | 60 | 40 | 10 | \ | Cocontinuous |
| 5 | 60 | 40 | \ | 5 | Sea–island |

* phr means per hundred parts of resins by weight.

### SEM characterization

SEM experiment was carried out to examine the phase morphology. The samples were fractured in liquid nitrogen and etched. The etched surfaces were then gold coated and investigated with an SEM instrument, JEOL JSM-5900LV SEM (Jeol JSM-5900LV, Tokyo, Japan), using an acceleration voltage of 20 kV. For overseeing the morphology of blends two etched methods, namely chemical etching and physical etching, were used to make contrast among PPS, PA66, and clay. For PPS/PA66 binary blends, the chemical etching was performed by immersion of the fractured specimens in formic acid (10 min, room temperature), which will dissolve the PA66 phase selectively. For the PPS/PA66/clay ternary composite, the physical etching was carried out, in which the fractured surface of the specimen was subjected to argon ion bombardment at 500 eV. The ion beam was focused perpendicularly to the surface of the specimens. Depending on the different resistance of the components to the ion beam etch (clay > PPS > PA66), the phase morphology and the location of the clay can be distinguished by this method.[21]

### Morphological characterization via dissolution experiments and quantitative extraction

The cocontinuous degree of the sample was estimated by the dissolution experiments. Some small pieces of the samples (about 0.05 $cm^3$) were immersed into formic acid at room temperature. Formic acid is a solvent for PA66 and a nonsolvent for PPS. The weights of the sample before and after extraction were measured to determine the loss weight of PA66 that was dissolved. It can be thought that in the sea–island structure, only PA66 at the surface can be extracted. And if a fully cocontinuous phase network is formed, all of the PA66 phase will be extracted by selective dissolution because all material is interconnected. In practice, however, the fully cocontinuous phase network is seldom encountered. The percentage of cocontinuity of the PA66 phase was then determined by the ratio of the weight of PA66 dissolved over the total weight of PA66 added to the blend. According to the data we got from the SEM, the clay is supposed to be located in the PA66 phase.

### Contact angle measurement

Contact angles were measured with KRUSS DSA100 Drop Shape Analyzer. Contact angles were measured on 3 mL of wetting solvent, and the results reported were the mean values of 10 replicates.

### XRD analysis

XRD analysis was performed by a Rigaku Denki RAD-B (Tokyo, Japan) with Cu Kα (λ = 0.154 nm) radiation at room temperature. The basal spacing of clay tactoid was estimated from the 001 peak in the XRD patterns.

### Rheometry

Rheological properties were determined with a capillary rheometer in shear rate region of $10^1$–$10^3$ $s^{-1}$ at 290°C. The capillary has a diameter of 1 mm and length of 10 mm.

### Mechanical properties

The tensile strength and tensile modulus were measured using a Shimadzi AG-10TA Universal Testing machine with a speed of 20 mm/min. Each mechanical test was repeated at least five times, and the results were averaged. For impact strength measurements, the notched specimens were tested with an I200XJU-2.75 impact tester at room temperature. Each mechanical test was repeated at least five times, and the results were averaged.

### Friction and wear testing

The friction and wear tests were conducted on a MM-200 friction and wear tester (Shanghai, China) at room temperature according to GB3960-83. The diameter of the steel ring (45#steel) is 40 mm, and the surface roughness (Ra) is 0.015 μm. The dimension of the specimen is 30 × 6 × 7 $mm^3$. The rotation speed of the steel ring is 200 rpm (load: 20 kg; time: 30 min) or 400 rpm (load: 10 kg, time: 30 min) during operation. Friction torques ($T$) was recorded every 5 min, and the friction coefficient was calculated by the equation given as follows:

$$\mu_\alpha = \frac{T_\alpha}{MR} \tag{1}$$

where $\mu_\alpha$ is the average friction coefficient, $T_\alpha$ the average friction torque (Kg cm); $M$ the load (kg); $R$ the radius of the steel ring (cm). Wear scar width of specimens was adopted to evaluate the antiwear property. Three replicate tests were carried out for each specimen. Before the testing, the steel rings and the specimens were washed with acetone and dried naturally.

## RESULTS AND DISCUSSION

### Morphological observation

PPS is an engineering plastic with high performances. Because of the poor impact property and high price, it often blends with PA66. Although the solubility parameter of two polymers is similar, they keep immiscible.[15] The phase morphologies of the PPS/PA66 (60/40 wt %) blends without and with different amounts of organic clay (1, 5, and 10 phr) are shown in Figure 1. All the pictures on the left are viewed along the flow direction, and the rights are viewed perpendicular to the flow direction. The PA66 phase was extracted by formic acid and shown as dark areas in the photos. One observes a typical sea–island structure for PPS/PA66 blend without clay [Fig. 1(a), right]. The PA66 spherical domains are dispersed in the PPS matrix because of its lower volume content in the blends. And the average diameter is about 1 μm. The PA66 phase is elongated along the flow direction due to the shear force. And the average length is about 4 μm. So, the PA66 is dispersed in the PPS matrix like oval-shaped sphere, and the $L/D$ is about four. By adding 1 phr organic clay, the situation is changed greatly. As shown in Figure 1(b) (left), the PA66 appears a layerlike structure. The layer length is much greater than 40 μm (the largest vision field of the photo), which is 10 times larger than 4 μm. It seems that PA66 forms a run-through layer along the flow direction. As viewed perpendicular to the flow direction, the PA66 phases are connected with each other, shown as a continued structure. At the same time, PPS also keeps a continue structure, thus a cocontinuous morphology is formed. The morphology is the typical oriented cocontinuous structure, which is elongated along the flow direction. In this case, both PPS and PA66 phases have isotropic three-dimensional spatial continuity in the composite. Increasing the content of organic clay, as shown in the Figure 1(c,d), the PA66 phase becomes thicker and bigger, and a lamellar supramolecular structure is formed. The effect of organic clay on the morphology of PPS/PA66 blends can be schematically represented in the Figure 1(e) with 3D view.

These micrographs clearly show the transition from a sea–island structure to a cocontinuous

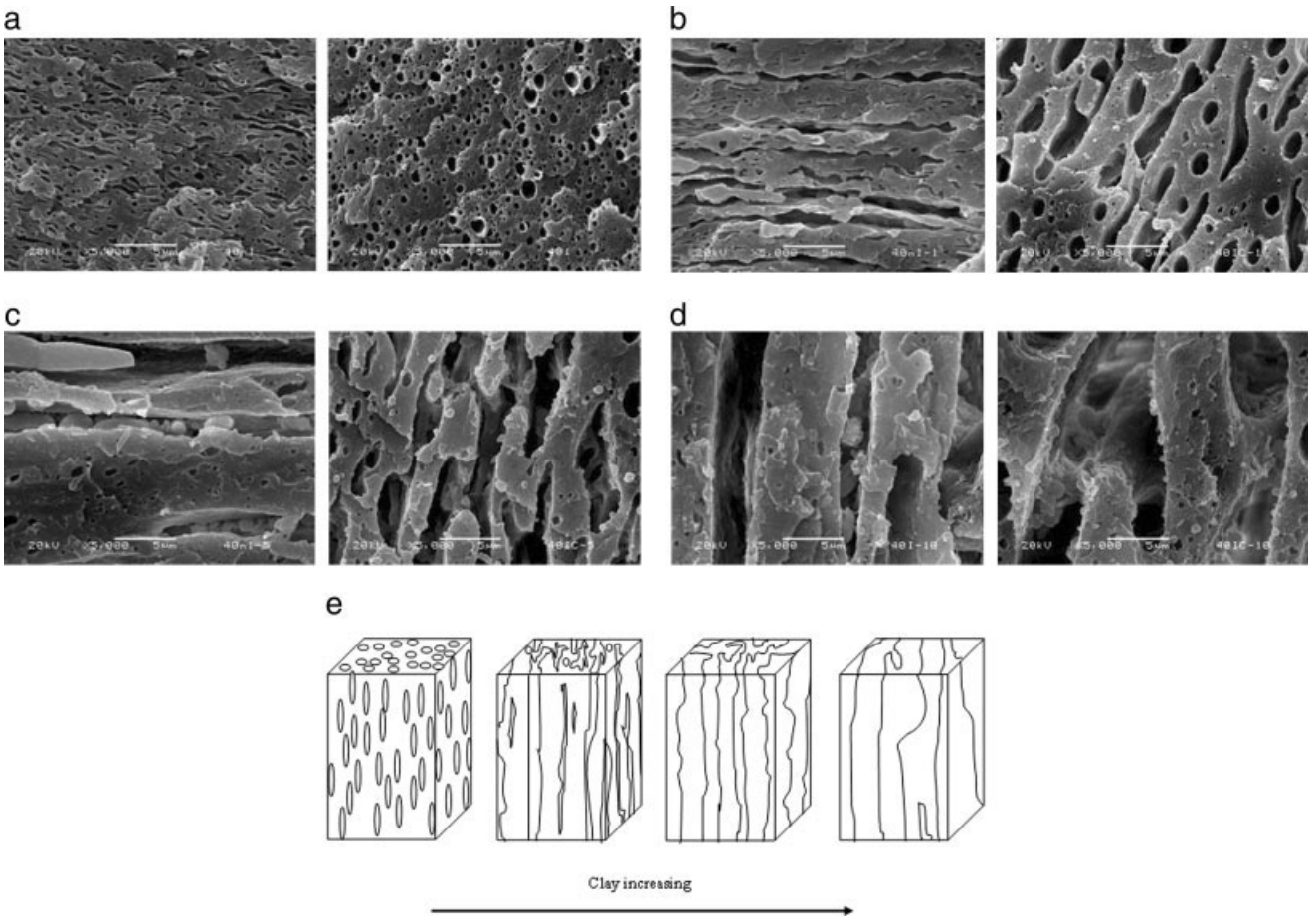


**Figure 1** SEM photos of composites with varying clay content. Left is along the injection direction and right is cross section: (a) without clay; (b) with 1 phr clay; (c) with 5 phr clay; (d) with 10 phr clay; (e) sketch of 3D morphology of each content.

morphology with large, interpenetrating structures. However, SEM does not always provide the complete information about the blend phase morphology because of its 2D feature. Therefore, the quantitative extraction experiments were performed as well to calculate the degree of cocontinuous structure.[23] For the extraction tests, about 3 g samples was put in formic acid for 72 h at room temperature to extract the PA66 phase. The weights of the sample before and after extraction were measured to determine the weight of PA66 that could be dissolved. The percentage of cocontinuity of the PA66 phase was then determined by the ratio of the weight of PA66 dissolved over the total weight of PA66 added to the blend with an assumption that all clay was located in the PA66 phase as shown later.

Figure 2 shows the change of cocontinuous degree with different contents of clay, taken that the fully cocontinuous degree as one. It can be found that the cocontinuous degree has a leap with 1 phr clay. Then the increase of the clay content results in a linear increase of the degree of cocontinuous. Finally, it reaches to 0.8, which is close to the fully cocontinuous morphology. This result indicates once again a systematic change of the phase morphology with increasing of clay content.

### Viscosity ratio characterization

It should be noted that the observed change of phase morphology in PPS/PA66 by adding organic clay is different from that reported in the literature. No lamellar supramolecular structure has been reported before. For better understanding, the change of the viscosity ratio was first checked. The melt viscosity of PPS (solid line) and PA66 (dash line) at 290°C as a function of shear rate is shown in Figure 3. From the data, it is seen that the viscosity of PPS is decreased with increasing of organic clay content,

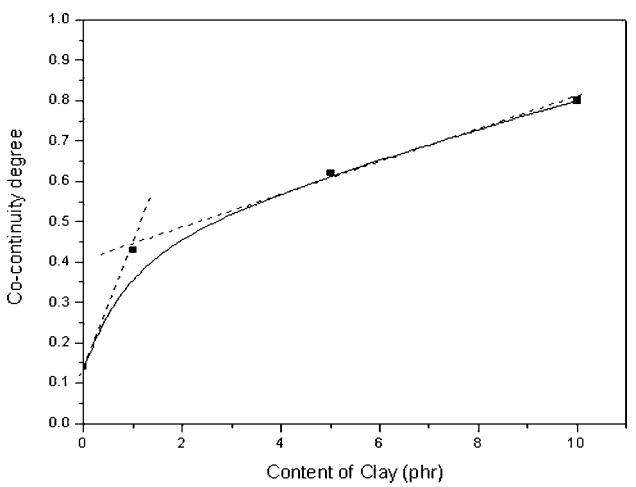


**Figure 2** Cocontinuous degree versus clay content.

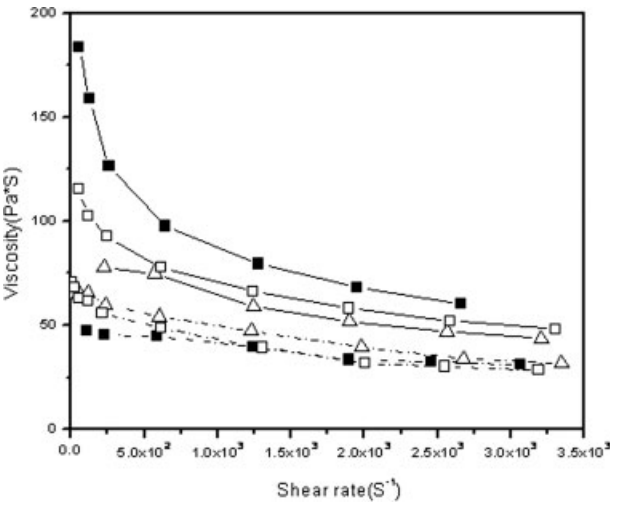


**Figure 3** The melt viscosity of PPS (solid line) and PA6,6 (dash line) at 300°C as a function of shear rate. Solid square: without clay; hollow square: with 1 wt % clay: hollow triangle: with 10 wt % clay.

while the viscosity of PA66 is increased slightly by adding organic clay. So, the viscosity ratio of PA66/PPS will increase by adding organic clay, indicating that the minor phase PA66 will easier to form the dispersed phase and PPS to form the matrix for PPS/PA66/clay ternary composite compared with the PPS/PA66 binary blends at the same composition. This is in contrary with the experimental observation. Thus, there must be other reason for the observed morphological change.

### Dispersion and location of clay

Before going step further, two factors should be made clear first. One is the structure of clay in the blends. Basically, three main types of composites may be obtained when layered clay is associated with a polymer namely phase separated, intercalated, and exfoliated structure. Many research results have indicated that only clay exfoliates into higher $L/D$ ratio single layers can a great enhancement of properties be expected, resulting from the strong interface interaction between polymer and clay. Figure 4(a) shows the WAXD profiles of the pure organic clay and the selected polymer/clay composites. The 001 diffraction of pure organic clay is at $2\theta = 2.5^\circ$, which corresponds to a $d$-spacing of 3.5 nm. In the PPS/PA66/clay and PA66/clay composite, no peak could be found, suggesting that parallel stacking of the nanofiller is totally disrupted. Oppositely, there is small peak still left in the PPS/clay composite at $2\theta = 6.5^\circ$, suggesting that some clay are still stacked together and not exfoliated. In fact, the exfoliated and intercalated structure has been reported in PA66/clay nanocomposites,[24–26] but only limited

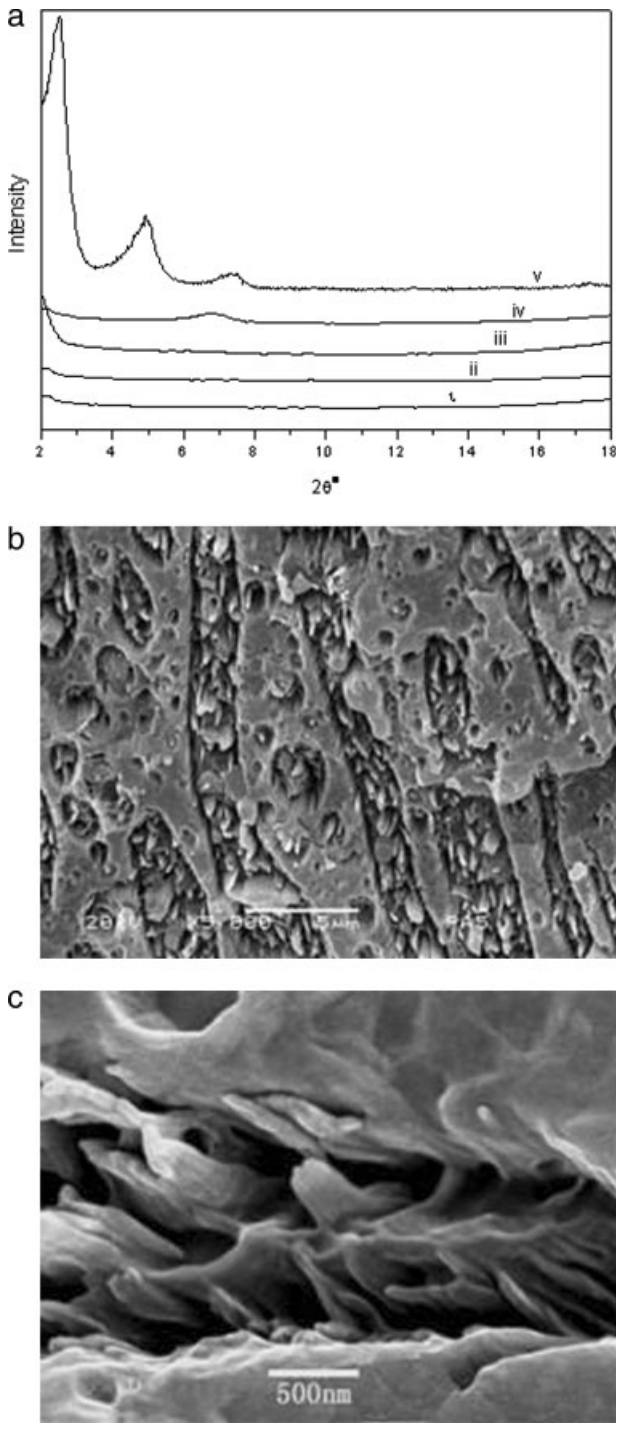


**Figure 4** (a) WAXD patterns (i), (ii), (iii) corresponding with blend contained 1, 5, and 10 phr clay respectively, (iv) PPS/clay composites, and (v) is pure clay; (b) SEM photo of PPS/PA66/clay composites (5 phr clay) after ion beam etched; and (c) SEM photo of the same sample in (b) with a higher magnification.

intercalation was seen in the PPS/clay composites,[27] which were in accordance with our WAXD result.

The second factor is the location of clay in the blend. To make clearer the location of clay, a new etching method named ion beam etching was introduced depending on the different resistance of the components to the ion beam. Figure 4(b,c) shows the SEM photos after ion beam etched. The PA66 phase is darker than the PPS phase, and the clay layers can also be seen clearly in this way. In the low magnification, it can be found that all clay is located in the PA66 phase exclusively though the subtle microstructure of clay cannot be distinguished clearly even under a relative high magnification [Fig. 4(c)].

The equilibrium morphology and the location of the filler within two-phase matrix formed by PPS and PA66, in principle, are determined through the interfacial forces of thermodynamic origin and wet ability of clay particles toward PPS and PA66. In practice, an equilibrium distribution may not be achieved since the kinetic issues can play a role in some circumstances.[28] From a thermodynamic point of view, the location of clay particles is determined by the following conditions[29]:

| | | |
|---|---|---|
| **a** | $\gamma_{p1f} > \gamma_{p2f} + \gamma_{p1p2}$ | The particle is completely immersed in polymer 2 |
| **b** | $\gamma_{p2f} > \gamma_{p1f} + \gamma_{p1p2}$ | The particle is completely immersed in polymer 1 |
| **c** | $\gamma_{p1f} < \gamma_{p2f} + \gamma_{p1p2}$ | The particle is located on the boundary polymer 1 and polymer 2 |
| | $\gamma_{p2f} < \gamma_{p1f} + \gamma_{p1p2}$ | |

where $\gamma_{p1f}$, $\gamma_{p2f}$, and $\gamma_{pp}$ are the interface surface tension of polymer 1-filler, polymer 2-filler, and polymer–polymer, respectively, assuming that the melt viscosities of polymer components are identical. The values of $\gamma_{p1f}$, $\gamma_{p2f}$, and $\gamma_{p1p2}$ can be calculated from the Fowkes equation:

$$\gamma_{12} = \gamma_1 + \gamma_2 - 2(\gamma_1\gamma_2)^{0.5} \quad (2)$$

in which $\gamma_{12}$ is interfacial tension, $\gamma_1$ and $\gamma_2$ are surface tension of components 1 and 2, respectively.

The surface tensions of PPS, PA66, and organic clay were measured with KRUSS DSA100 Drop Shape Analyzer. The results are listed in Table II. It can be concluded as

**TABLE II**
**Surface and Interface Tensions of Components of the Blends**

| | $\gamma$ (mN/m) |
|---|---|
| PPS | 44.01 |
| PA66 | 42.94 |
| Clay | 26.03 |
| PPS/PA66 | 0.00658 |
| PPS/clay | 2.35 |
| PA66/clay | 2.11 |

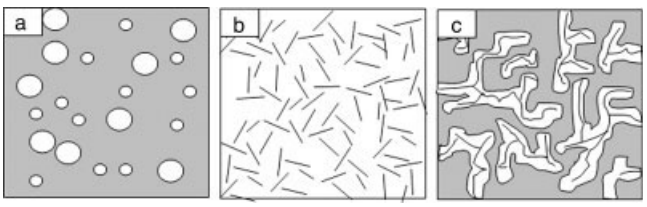


**Figure 5** Self-assembly of rods into a percolating network: (a) the A/B mixture without rods; (b) rods without fluid; and (c) rods and A/B mixture after long time evolution. White regions are A domains, gray regions are B domains, and dark lines in the white areas depict rods.

$$\gamma_{PPS-clay} = 2.35 \text{ mN/m} \geq \gamma_{PA66-clay} + \gamma_{PA66-PPS}$$
$$= 2.11658 \text{ mN/m}$$

According to the result of surface tension, clay can be more likely to be located in the PA66 phase than in the PPS phase. This is in good agreement with the experimental observation.

### Formation of supramolecular networks from nanoscale rods

Now let us check the clay network induced self-assemble theory proposed by Balazs and coworkers[30] using computer simulations. Their results indicated that when low-volume fractions of nanoscale rods were immersed in a binary, phase-separation blend, the rods self-assemble into a needlelike, percolating network. The interconnected network arose through the adsorption of the minority component onto the mobile rods, and through rod–rod repulsion (Fig. 5). The simulation was supported by the works of Krishnamoorti's group, who did much work on the nanofiller effect on the polystyrene and poly(vinyl methyl ether) blend films.[31] They found that the blends with small disk diameter (30 nm and 0.5 μm) nanoparticles exhibited a pinning of domain sizes and demonstrated an increase in the number of domains with a higher fraction of near circular structures and the extent of domain pinning increased with increasing silicate content, resulting in smaller domains at higher concentrations of silicate. They used ''domain pinning'' instead of ''network'' for their works performed in the film. Here, in PPS/PA66/clay system, a network of the exfoliated clay layers is most likely to be formed in PA66 matrix since the clay layers are seen to stack each other [Fig. 4(c)]. The formation of clay layers' network has been reported in many polymer/clay systems.[32–35] Since the clay is seen to locate only in the PA66 phase, its content in this phase will be double, which increases the possibility for the formation of clay network. Thus, the formation of supramolecular networks can be tentatively explained as follows: due to the dynamic interplay of phase-separation between PPS and PA66, and preferential adsorption of PA66 onto the clay layers and through layer–layer repulsion, the formation of clay network will direct association of the PA66 phase into the cocontinuous supramolecular structure [Fig. 1(b)]. By simulation, Balazs estimated that there exists a critical density of rods that is needed to effectively form a percolating network. If the clay content is larger than the critical density, there exists a range of number density for which the system self-assembles into the morphology of microphase-separated diblock copolymer, lamellar supramolecular structure [Fig. 1(c)]. However, if the number density is increased significantly beyond the critical density, this lamellar morphology is destroyed [Fig. 1(d)], because too many clay layers to be accommodated in the PA66 phase and forced into the PPS phase.

Now it is turned out that whether or not existing exfoliated clay is the key issue for the observed morphological change. To prove this, an experiment was conducted to obtain unexfoliated clay in PPS/PA66 blends by using untreated clay. The corresponding WAXD and SEM results are shown in Figure 6. In this case, no more cocontinuous structure is observed, as shown in Figure 6(a). Viewed perpendicular to the flow direction [Fig. 6(a), right], the PA66 phase exhibits sphere structure, and the average diameter is 2.4 μm, which is bigger than that for the blends without clay. Viewed along the flow direction [Fig. 6(a), left], the PA66 phase is elongated, and the average length is 16 μm. To combine the structure in two directions, PA66 morphology in the composites is cylinder with 6.7 $L/D$ ratio. WAXD result [Fig. 6(b)] and SEM photo of ion-etched sample [Fig. 6(c)] all indicate that the untreated clay has not exfoliated. So only exfoliated clay that selectively located in PA66 phase can change the phase morphology from sea–island into cocontinuity and a lamellar structure occurs.

### Mechanical properties

The mechanical properties of PPS/PA66 blends with different contents of clay are shown in Figure 7, in which the variability of data is within ±7%. From this figure, it can be seen that the mechanical properties of PPS/PA66 are obviously improved by adding clay. The tensile strength of the blends shows increase of 10 MPa just by adding 1 wt % clay and elevates 15 MPa when the clay content goes to 5 wt %, which increases by 24 and 35% compared to the PPS/PA66 blend. At the same time, the impact strength is increased continuously with the increase in in clay amount.

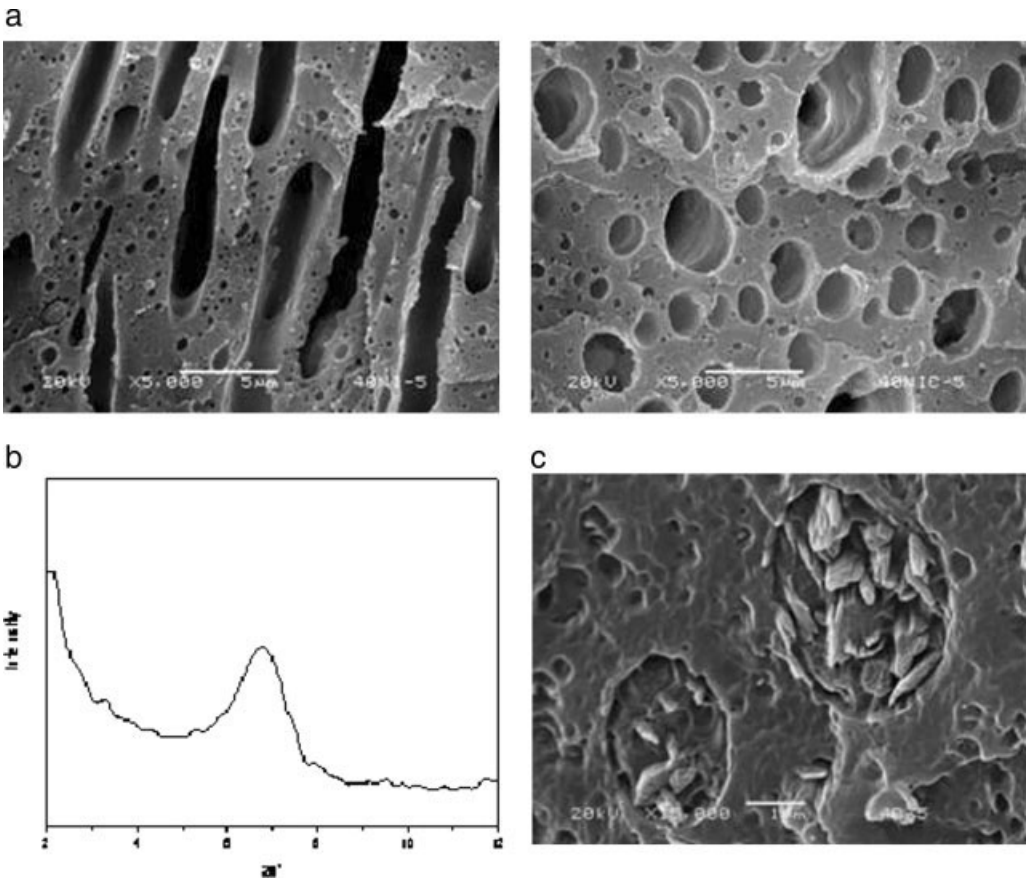


**Figure 6** (a) SEM photos of composites with 5 phr untreated clay. Left are along the injection direction and right are cross section; (b) WAXD pattern; (c) SEM photos after ion beam etched.

### Friction and wear behaviors of PPS and PA66 nanocomposites

To better understand the tribological properties of the PPS/PA66/clay system, we first investigated the tribological properties of the PPS/clay and PA66/clay composites, because some nanoparticles have showed an important effect on the tribological properties of polymers,[36,37] particularly at high content. The friction coefficients of PPS/clay and PA66/clay composites are shown in Figure 8. No change of friction coefficient for both PPS and PA66 by adding clay. The friction coefficients of PPS and composites keep around 0.65 under low speed and 0.87 under high speed. Similarly, PA66 keeps around 0.27 (low speed) and 0.45 (high speed). This result indicates that one can ignore the effect of clay on the tribological properties, and any changing in the tribological properties is resulted from the change of phase morphology.

### Friction and wear behaviors

Figure 9 reveals the friction coefficient of PPS/PA66/clay blends as function of clay content under the low-speed condition (200 rpm) and high-speed condition (400 rpm). The friction coefficients of PPS/PA66/clay blends keep unchanged until the clay content reaches to 10 phr, where a remarkably decrease of friction coefficient is observed for both low-speed condition and high-speed conditions. This is most likely caused by the lamellar supramolecular structure as one observes from the SEM experiment. On the other hand, for the blend with sea–island type (without clay), the friction coefficient is in the range between that of PPS and PA66. According to the simple adding law,

$$\mu_{\text{blends}} = \mu_{\text{PPS}}\varphi_{\text{PPS}} + \mu_{\text{PA66}}\varphi_{\text{PA66}} \tag{3}$$

where $\mu$ is the friction coefficient and $\varphi$ is the weight content of blends.

For example, at the low speed,

$$\mu_{\text{blends}} = 0.65 \times 60\% + 0.27 \times 40\% = 0.55.$$

It can be found that the theory data is in agreement with the experimental data. However, by adding clay, the morphology is changed from sea–island to cocontinuity, the friction coefficients of blends are

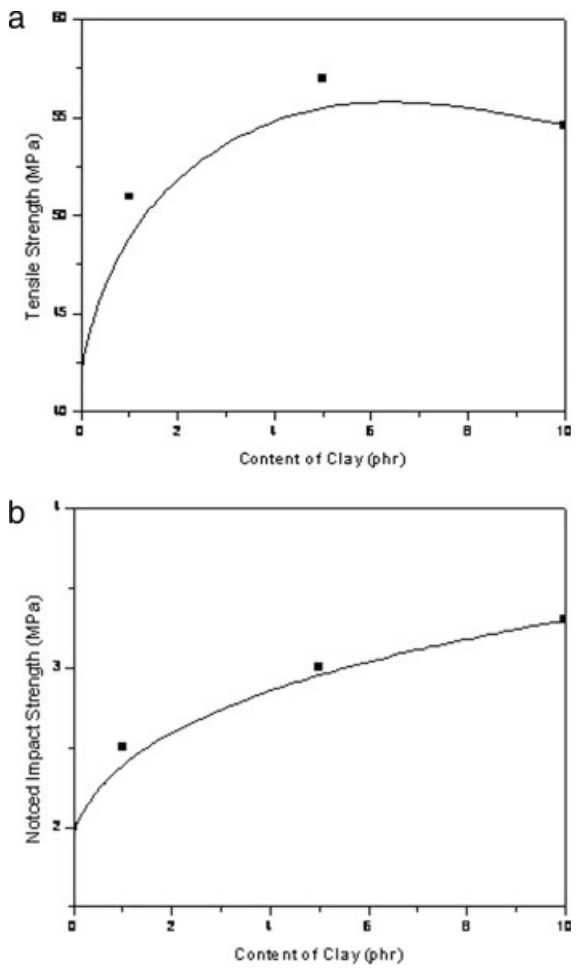


**Figure 7** Mechanical property of blends with varying clay content (a) tensile strength and (b)impact strength.

no more obeyed to the adding law and is close to the values of pure PA66 (even lower than it).

### Investigation of wear mechanism

The tribological properties of polymers and their composites are strongly influenced by their ability to form a transfer film on the counter face.[38] Once a transfer film is formed, subsequent interaction occurs between the polymer and a layer of similar material, instead of polymer and metal counter face. SEM is one of the powerful methods in research of friction and wear mechanisms in tribology to observe the worn surface. Therefore, the worn surfaces and the transfer films on the steel counter face formed by the PPS/PA66 and PPS/PA66/clay blends during sliding were examined with SEM.

#### Low speed

The micrographs of the counter-face sliding against PPS/PA66 without clay at low speed and the worn surface are given in Figure 10. For the immiscible blend system without clay, the worn surface is rough and exhibits some scratch grooves parallel to the sliding direction in the worn surface when sliding against the steel counterpart at low magnification [Fig. 10(a)]. From the images at higher magnification, it can be seen that nonuniform thin sheets are generated in the whole area investigated and thereby a rippled structure is formed, which is perpendicular to the sliding direction. Scalelike wear debris produced during sliding is shown in Figure 10(c). This result suggests that the polymer might be peeled off layer by layer from the sample during sliding. The SEM micrograph of transfer film formed by PPS/PA66 (60/40) blend is shown in Figure 10(d). A nonuniform and discontinuous transfer film on the surface of the steel ring is observed.

The PPS/PA66 (60/40) blend with 10 phr clay was selected for comparison and understanding of tribological properties versus phase morphology. There are many deformed layers on the worn surface. At

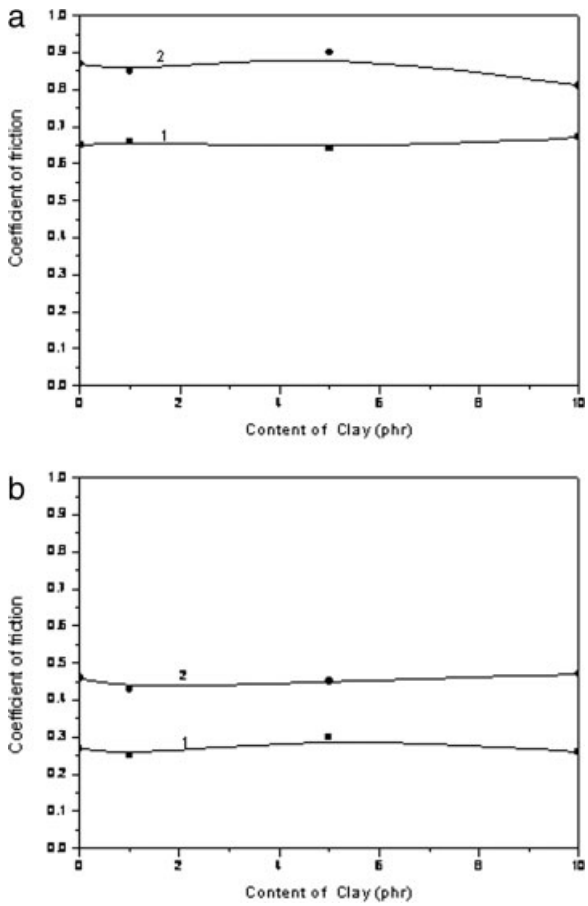


**Figure 8** Variation of coefficient of friction with clay contents in PPS and PA66 nanocomposites. (a) PPS with different contents of clay, (b) PA66 with different contents of clay, and (1) at low speed situation (speed: 200 rpm; load: 20 kg) and (2) at high speed situation (speed: 400 rpm; load: 10 kg).

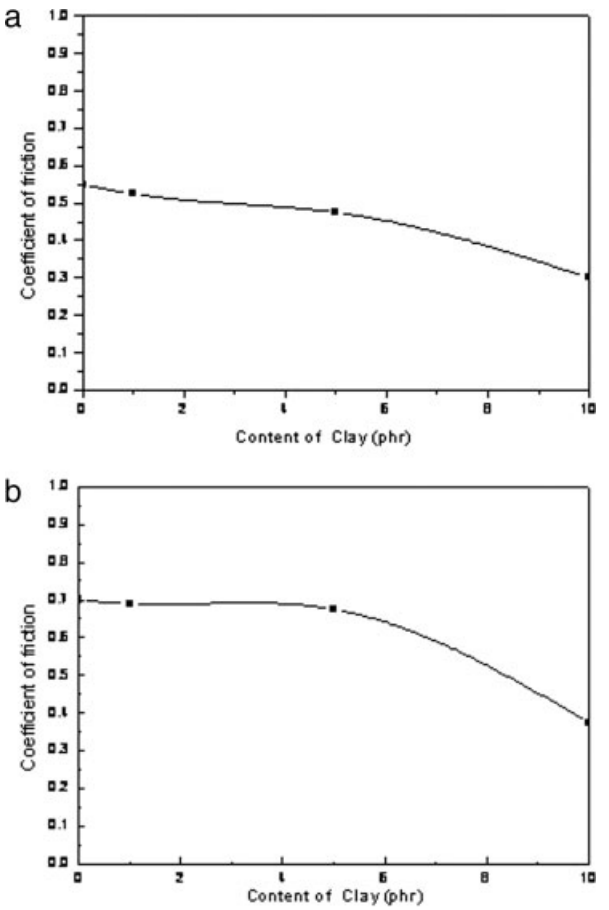


**Figure 9** Variation of coefficient of friction with clay contents in blends. (a) Low speed situation (speed: 200 rpm; load: 20 kg; time: 30 min); (b) high speed situation (speed: 400 rpm, load: 10 kg; time: 30 min).

higher magnification [Fig. 11(b)], it is seen that the scratch originates a lot of elongated sheets parallel to the sliding direction instead of obvious scratch grooves. Obvious plastic deformation is observed in the worn surface and polymer all flake away from the sample. The wear debris is changed from the layer to the fiberlike [Fig. 11(c)]. The wear debris blocks the direct contact between the steel and the blend matrix, acting as rolling lubricants. Therefore, the friction and wear properties of blends are improved effectively. It can be seen from Figure 11(d) that the contact surface seems to be covered by a lubricant film, which prevents the bulk from serious wear.

### High speed

Sequentially, the wear behavior of trinary PPS/PA66/clay composite is evaluated upon the high scratch speed. Under the high sliding speed, the effect of temperature on the worn surface should be considered due to the poor thermal conduction of polymers. The temperature of the worn surface can be increased quickly because of the produced friction heat.

The worn surface of PPS/PA66 with sea–island morphology shows deeper holes, which is characterized by adhesion and friction-heat induced softening and plastic deformation [Fig. 12(a,b)]. This conforms to poorer wear resistance of this blend. The agglomerate wear debris indicates an apparent melting trace [Fig. 12(c)]. The discontinued transferred film is brown and adheres firmly to the steel ring surface due to serious oxidization [Fig. 12(d)]. It is evident that the temperature at the sliding interface has reached its melting point of PA66 during sliding, resulting in a poor wear property.

When the morphology is changed into cocontinuous structure by adding clay, the deeper holes become into the long scratch grooves parallel to the sliding direction [Fig. 13(a,b)]. And the wear debris is changed from agglomerate to rodlike [Fig. 13(b)]. The transform film becomes more continue and thinner [Fig. 13(d)]. This all contributes to the lower friction coefficient.

Owning to the fact that the wear debris originating from the polymer surface has experienced complicated interaction of the steel counterpart, the different debris morphologies should correspond to different wear mechanisms. Generally, the granular particles including the rodlike and blocklike debris can be attributed to an abrasive microcutting effect. On the other hand, fatigue delamination is also an important wear mechanism, which is usually considered to be responsible for the debris in the form of sheets. It can be seen from above SEM observation that all fragments of wear debris exhibit different morphology. The wear debris of PPS/PA66 blend with clay (cocontinuous structure) exhibits lamellar structure and uneven edges, indicative of plastically stretching and resin melting duration formation [Fig. 13(c)]. This suggests that the formation of lubricant layer is just due to the molten of the wear debris. Because the melt point of PA66 is lower than that of PPS, the wear debris probably is resulted from the PA66 particles that have been pulled out of the specimen surface, and then oriented along the sliding direction to a certain extent under the frictional shear force. After a long time sliding it gradually melts and forms the lubricant layer in the worn surface. When the PA66 phase is droplike, the PA66 particles that been pulled out could not form sheet. In the contrast, the continued PA66 phase is in propitious to form the large sheet. By this mechanism, the transform film can be easily formed for the blends with cocontinuous phase structure. A stable, continued transform film is favor for improving the tribological properties.

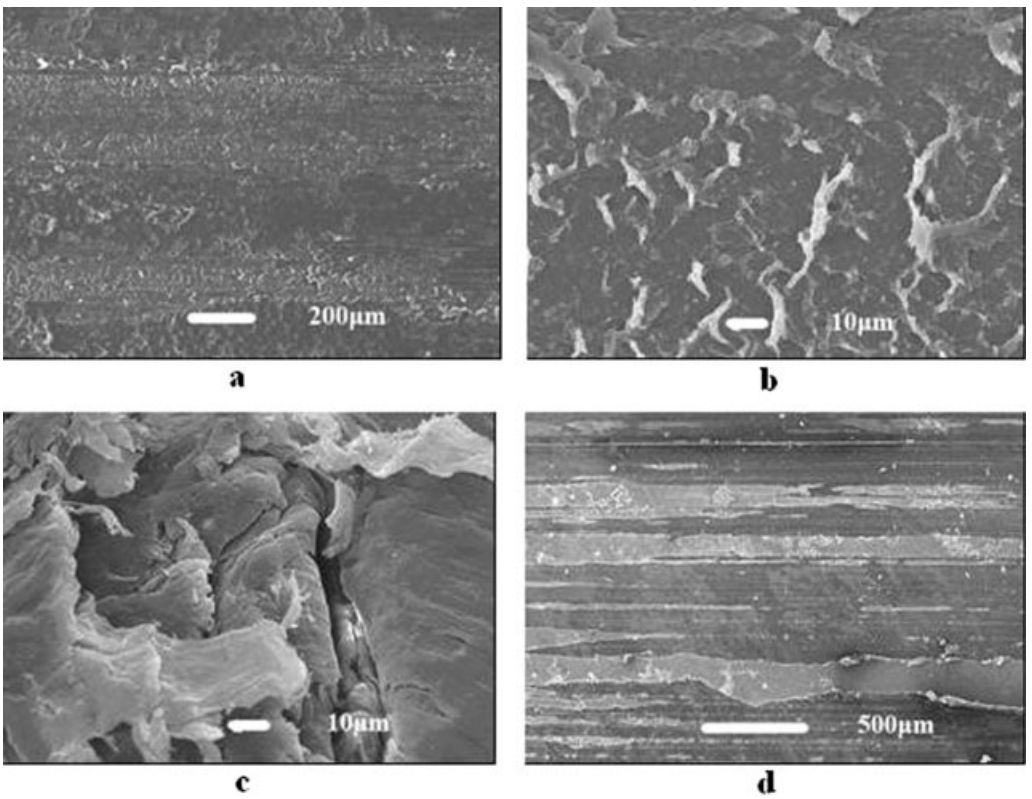


**Figure 10** Scanning electron micrographs of blends without clay at low speed (speed: 200 rpm, load: 20 kg; time: 30 min): (a) worn surface, (b) worn surface, (c) wear debris produced during sliding, and (d) steel counterpart surface sliding against blends.

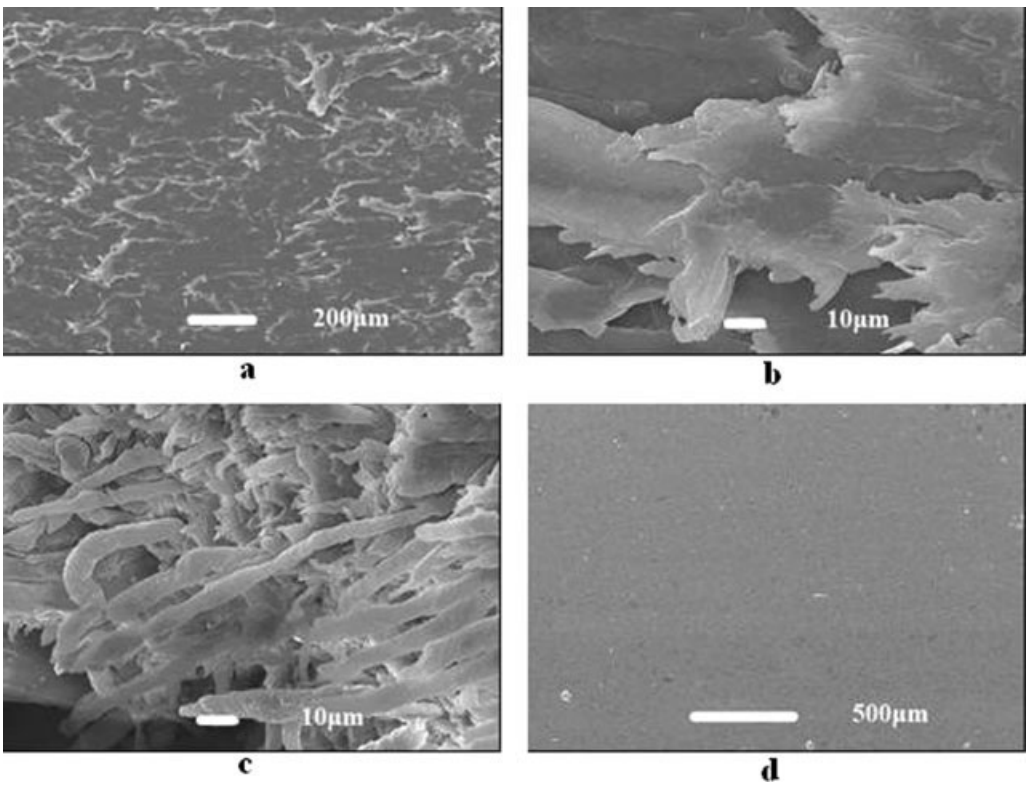


**Figure 11** Scanning electron micrographs of blends with 10 phr clay at low speed (speed: 200 rpm; load: 20 kg; time: 30 min): (a) worn surface, (b) worn surface, (c) wear debris produced during sliding, and (d) steel counterpart surface sliding against blends.

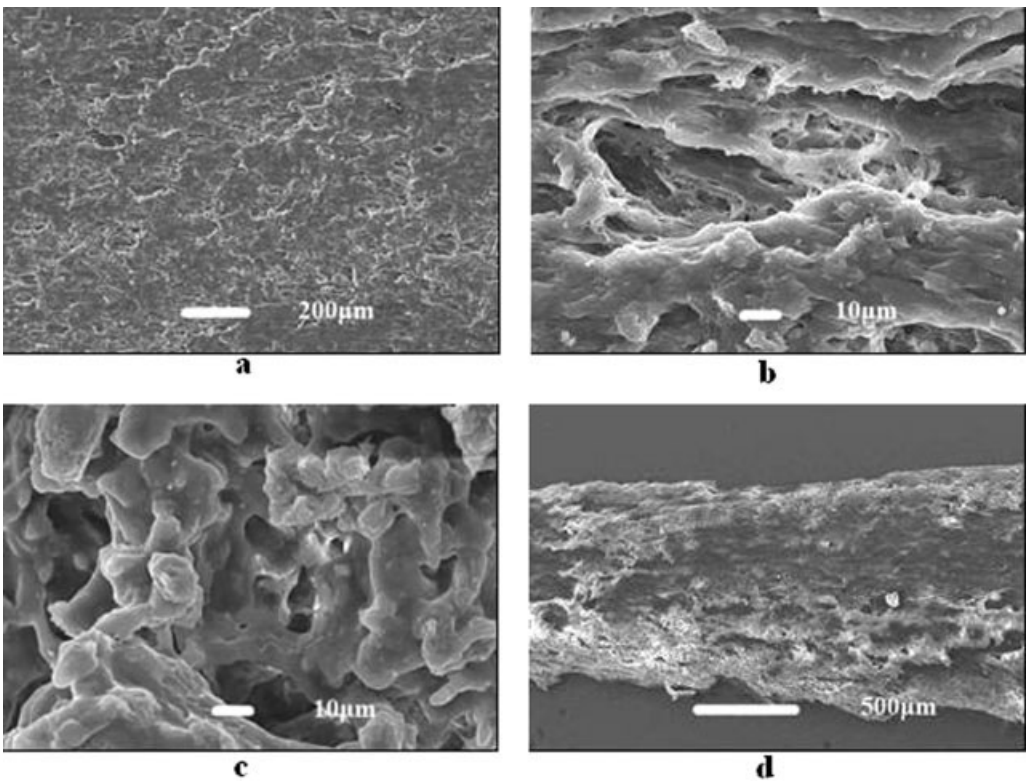


**Figure 12** Scanning electron micrographs of blends without clay at high speed (speed: 400 rpm; load: 10 kg; time: 30 min): (a) worn surface, (b) worn surface, (c) wear debris produced during sliding, and (d) steel counterpart surface sliding against blends.

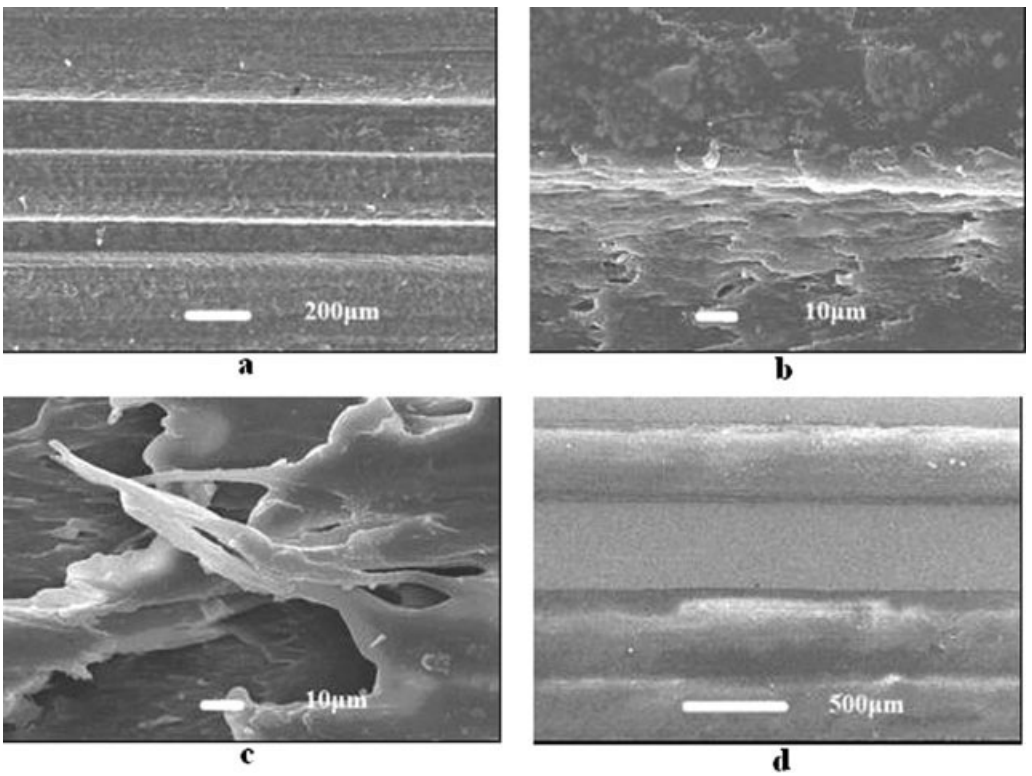


**Figure 13** Scanning electron micrographs of blends with 10 phr clay at high speed (speed: 400 rpm; load: 10 kg; time: 30 min): (a) worn surface, (b) worn surface, (c) wear debris produced during sliding, and (d) steel counterpart surface sliding against blends.

## CONCLUSIONS

The morphologies of PPS/PA66 blends with various amounts of clay have been investigated in this study. It is found that the clay is selectively located in the PA66 phase and the exfoliated clay layers form the edge-touched network structure. The inorganic network and the wetting of the PA66 phase on it are considered to induce self-assembly and finally form a supramolecular network. These make the composites morphology changed from sea–island to cocontinuity and lamellar structure. The mechanical properties are increased through adding clay. The blend with cocontinuous structure forms transform film easily and results in an outstanding improvement in the tribological properties. Our work provides a new way to create a rich diversity of new structures and useful nanocomposites.

## References


1. Pinnavaia, T. G.; Beall, G. W. Polymer-Clay Nanocomposites; Wiley: New York, 2000.
2. Alexandre, M.; Dubois, P. Mater Sci Eng 2000, 28, 1.
3. Fischer, H. Mater Sci Eng C 2003, 23, 763.
4. Ray, S. S.; Okamoto, M. Prog Polym Sci 2003, 28, 1539.
5. Wang, Y.; Zhang, Q.; Fu, Q. Macromol Rapid Commun 2003, 24, 231.
6. Ray, S. S.; Bousmina, M. Macromol Rapid Commun 2005, 26, 450.
7. Mehrabzadeh, M.; Kamal, M. R. Can J Chem Eng 2002, 80, 1083.
8. Khatua, B. B.; Lee, D. J.; Kim, H. Y.; Kim, J. K. Macromolecules 2004, 37, 2454.
9. Feng, M.; Gong, F. L.; Zhao, C. G.; Chen, G. M.; Zhang, S. M.; Yang, M. S. Polym Int 2004, 53, 1529.
10. Li, Y. J.; Shimizu, H. Polymer 2004, 45, 7381.
11. Li, Y. J.; Shimizu, H. Macromol Rapid Commun 2005, 26, 710.
12. Rafailovich, M.; Sokolov, J.; Zhu, S.; Chu, B. U.S. Pat. 6,339,121 (2002).
13. Cheng, S. Z. D.; Wunderlich, B. Macromolecules 1987, 20, 2802.
14. Brady, D. G. J Appl Polym Sci Appl Polym Symp 1981, 36, 23.
15. Akhtar, S.; White, J. L. Polym Eng Sci 1992, 32, 690.
16. Watanabe, M.; Yamaguchi, H. Wear 1986, 110, 379.
17. Chen, Y. K.; Kukureka, S. N.; Hooke, C. J.; Rao, M. J Mater Sci 2000, 35, 1269.
18. Bahadur, S.; Gong, D. Wear 1992, 154, 207.
19. Kukureka, S. N.; Hooke, C. J.; Rao, M.; Liao, P.; Chen, Y. K. Tribol Int 1999, 32, 107.
20. Zhao, Q.; Bahadur, S. Wear 1999, 225, 660.
21. Chen, Z. B.; Li, T. S.; Yang, Y. L.; Liu, X. J.; Renguo, L. V. Wear 2004, 257, 696.
22. Usuki, A.; Okamoto, T. Nano Lett 2001, 1, 271.
23. Tol, R. T.; Groeninckx, G.; Vinckier, I.; Moldenaers, P.; Mewis, J. Polymer 2004, 45, 2587.
24. Mehrabzadeh, M.; Kamal, M. Polym Eng Sci 2004, 44, 1152.
25. Chavarria, F.; Paul, D. R. Polymer 2004, 45, 8501.
26. Lu, Y. L.; Zhang, Y.; Zhang, G. B.; Yang, M. S.; Yan, S. K.; Shen, D. Y. Polymer 2004, 45, 8999.
27. Zou, H.; Xu, W.; Zhang, Q.; Fu, Q. J Appl Polym Sci 2006, 99, 1724.
28. Mamunya, Y. Macromol Symp 2001, 170, 257.
29. Mamunya, Y. J Macromol Sci Phys 1999, 38, 615.
30. Peng, G. W.; Qiu, F.; Ginzburg, V. V.; Jasnow, D.; Balazs, A. C. Science 2000, 288, 1802.
31. Galgali, G.; Ramesh, C.; Lele, A. Macromolecules 2001, 34, 52.
32. Yurekli, K.; Karim, A.; Amis, E. J.; Krishnamoorti, R. Macromolecules 2003, 36, 7256.
33. Hoffman, B.; Mulhaupt, R. Macromol Rapid Commun 2000, 21, 57.
34. Ren, J.; Silva, A. S.; Krishnamoorti, R. Macromolecules 2000, 33, 3739.
35. Ray, S. S.; Maiti, P.; Okamoto, M.; Yamada, K.; Ueda, K. Macromolecules 2002, 35, 3104.
36. Zhao, Q.; Bahadur, S. Wear 1998, 217, 62.
37. Schwartz, C. J.; Bahadur, S. Wear 2000, 237, 261.
38. Bahadur, S. Wear 2000, 245, 92.